A Comparative Study of Cellular Uptake and Subcellular Localization of Doxorubicin Loaded in Self-Assemblies of Amphiphilic Copolymers with Pendant Dendron by MDA-MB-231 Human Breast Cancer Cells

Geetha Viswanathan, Yu-Hsuan Hsu, Siew Hui Voon, Toyoko Imae,* Ampornphan Siriviriyanun, Hong Boon Lee, Lik Voon Kiew, Lip Yong Chung,* Shin-ichi Yusa

Previously synthesized amphiphilic diblock copolymers with pendant dendron moieties have been investigated for their potential use as drug carriers to improve the delivery of an anticancer drug to human breast cancer cells. Diblock copolymer ($P_{71}D_3$)-based micelles effectively encapsulate the doxorubicin (DOX) with a high drug-loading capacity (≈95%, 104 DOX molecules per micelle), which is approximately double the amount of drug loaded into the diblock copolymer ($P_{296}D_1$) vesicles. DOX released from the resultant $P_{71}D_3$/DOX micelles is approximately 1.3-fold more abundant, at a tumoral acidic pH of 5.5 compared with a pH of 7.4. The $P_{71}D_3$/DOX micelles also enhance drug potency in breast cancer MDA-MB-231 cells due to their higher intracellular uptake, by approximately two-fold, compared with the vesicular nanocarrier, and free DOX. Micellar nanocarriers are taken up by lysosomes via energy-dependent processes, followed by the release of DOX into the cytoplasm and subsequent translocation into the nucleus, where it exert its cytotoxic effect.

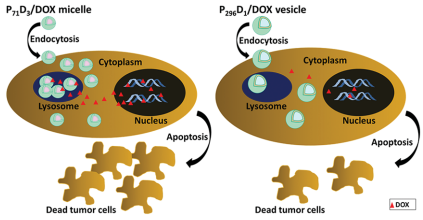

Dr. G. Viswanathan, Dr. H. B. Lee, Prof. L. Y. Chung
Department of Pharmacy
Faculty of Medicine
University of Malaya
50603 Kuala Lumpur, Malaysia
E-mail: chungly@hotmail.com
Y.-H. Hsu, Prof. T. Imae
Department of Chemical Engineering
National Taiwan University of Science and Technology
43 Section 4, Keelung Road, Taipei 10607, Taiwan
E-mail: imae@mail.ntust.edu.tw
S. H. Voon, Dr. L. V. Kiew
Department of Pharmacology
Faculty of Medicine
University of Malaya
50603 Kuala Lumpur, Malaysia
Prof. T. Imae, Dr. A. Siriviriyanun
Graduate Institute of Applied Science and Technology
National Taiwan University of Science and Technology
43 Section 4, Keelung Road, Taipei 10607, Taiwan
Dr. S.-i. Yusa
Department of Materials Science and Chemistry
University of Hyogo
2167 Shosha, Himeji, Hyogo 671–2280, Japan

Macromol. Biosci. **2016**, *16*, 882–895

DOI: 10.1002/mabi.201500435

1. Introduction

Micelles and vesicles have been developed as promising colloidal carriers for the delivery of anticancer drugs to tumor cells. Surfactants, synthetic and natural polymers, lipoproteins, liposomes, and amphiphilic polymer based micellar systems have been extensively studied for this purpose.[1] Surfactant micelles are commonly used as drug carriers but suffer from thermodynamic and kinetic instability upon extreme dilution following intravenous administration due to their high critical micelle concentration.[2] They are also associated with toxicity and tolerability issues. For instance, cremophor EL micelles administered intravenously were found to cause adverse effects, including severe anaphylactic hypersensitivity reactions, hyperlipidemia, lipoprotein structural abnormalities, and peripheral neuropathy.[3] Lipoproteins, which could be recognized by healthy cells, compete with natural lipoproteins for receptor sites on tumors.[4] Liposomes, on the other hand, possess inherent weaknesses, such as low encapsulation efficiency, poor stability in systemic circulation and rapid clearance by the reticuloendothelial system.[5] Among drug carriers, amphiphilic polymeric micelles and vesicles have the advantages of small particle sizes, high drug encapsulation capacities, hydrophilic surfaces that prevent opsonization and passively accumulate in tumors due to the enhanced permeability and retention effect.[6] However, these polymeric nanocarriers must be further improved in terms of drug-loading efficiency, stability in the systemic circulation after injection, and transportability through the cell membrane for uptake by tumor cells.[7]

Amphiphilic diblock copolymers are mainly used for the preparation of polymeric aggregates.[6b] These diblock copolymers can self-assemble into two different forms in aqueous solutions as follows: core–shell spherical micelles or vesicles, depending on the hydrophobic/hydrophilic balance.[8] Our group synthesized an amphiphilic diblock copolymer ($P_{71}D_3$) consisting of a linear polyelectrolyte block and a hydrophobic block carrying a

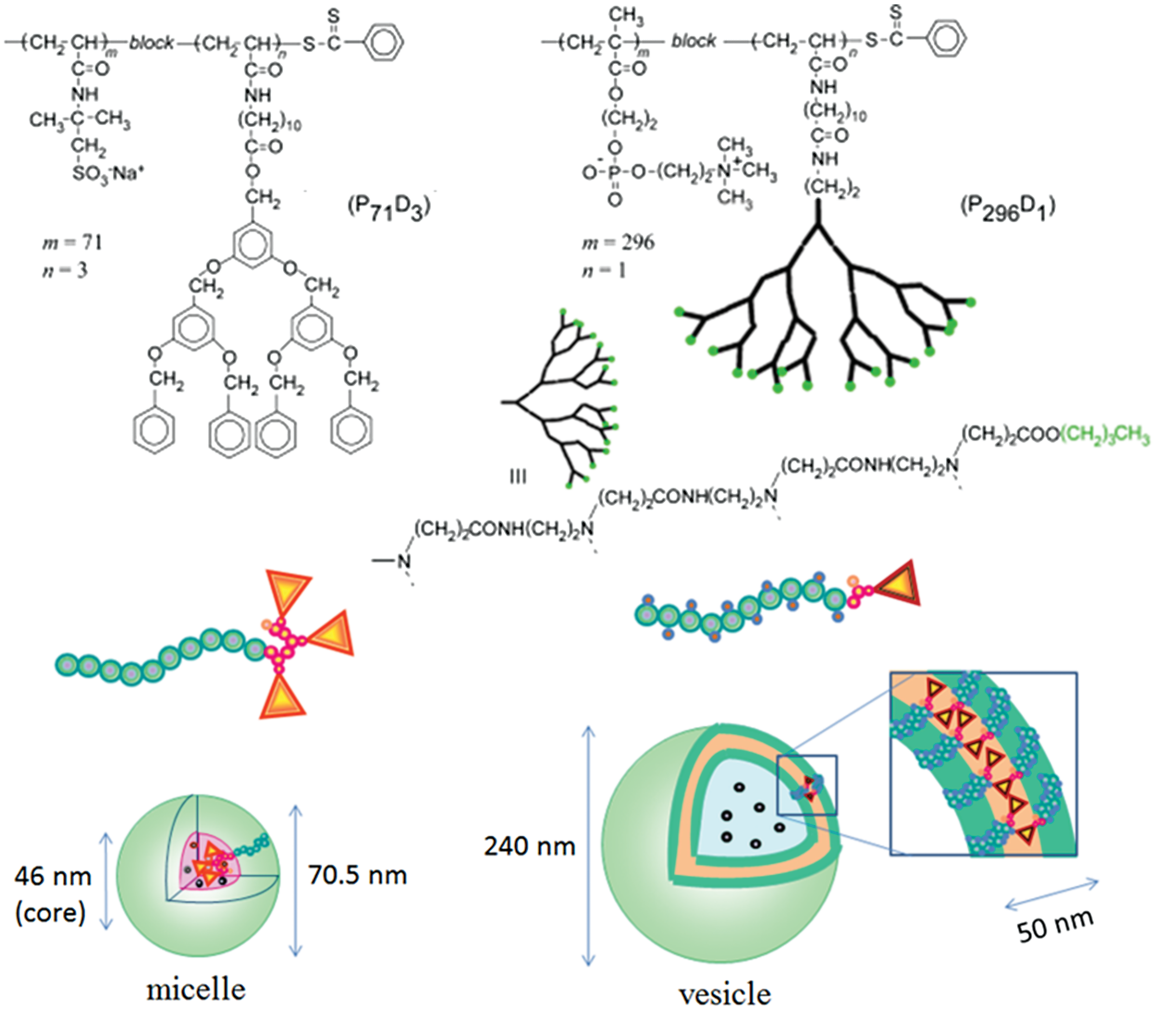

Scheme 1. Chemical structures of $P_{71}D_3$ and $P_{296}D_1$; schematic representation of their self-assemblies.

pendant benzyloxy-type dendritic moiety[9] (Scheme 1). This polymer self-aggregates into spherical micelles of 70.5 nm diameter with a narrow size distribution, and the polymer micelles are able to entrap hydrophobic guest molecules into the large cavity or available void, within and between the hydrophobic dendron moieties in the micelle core.[10]

Another amphiphilic diblock copolymer was composed of a hydrophilic pendant phosphorylcholine moiety and hydrophobic amido amine-type dendron side chain moiety.[11] The polymer ($P_{296}D_1$) formed vesicles in water, which was mostly likely due to its rod-like shape, with side chains on both blocks (Scheme 1). In this case, the vesicles were able to accommodate hydrophilic guest molecules in the interior water pool of $P_{296}D_1$ vesicles.

In this study, micellar and vesicular self-assemblies consisting of two diblock copolymers ($P_{71}D_3$ and $P_{296}D_1$, respectively) were assessed for their ability to load and release the anticancer drug, doxorubicin (DOX), and were also evaluated for their effects on the viability and intracellular uptake efficiency of MDA-MB-231 human breast cancer cells to determine their potential as nanocarriers for drug delivery. Incidentally, since DOX is soluble in water but possesses an aromatic moiety, it is amphiphilic and can exist in both hydrophilic and hydrophobic environments. Therefore, it can be encapsulated in the hydrophobic micellar core and the hydrophilic water pool in vesicles.

2. Experimental Section

2.1. Materials

N-hydroxysuccinimide (NHS) and *N*,*N*′-dicyclohexylcarbodiimide were purchased from ACROS (Morris Plains, NJ, USA). Fluoresceinyl glycine amide (FGA) was purchased from Thermo Fisher Scientific (Waltham, MA, USA). DOX was kindly donated by Prof. H. C. Tsai, National Taiwan University of Science and Technology, Taiwan. Various fluorescent dyes and trackers such as ProLong Gold Antifade Mountant with DAPI, ER-Tracker Blue-White DPX (E-12353), LysoTracker Blue DND-22 (L-7525), MitoTracker Red FM (M-22425), and MitoTracker Green (M-7514) were purchased from Molecular Probes, Invitrogen (Eugene, OR, USA). Other reagents were commercially available. Deionized ultrapure (ELGA PURELAB flex 3) water with a resistivity of 18.2 MΩ·cm was used throughout all syntheses and measurements.

The diblock copolymers $P_{71}D_3$ and $P_{296}D_1$ (see Scheme 1) were the same samples as those previously synthesized.[9,11] Micelles (hydrodynamic diameter: 65 nm, transmission electron microscopic (TEM) diameter: 70.5 nm) of $P_{71}D_3$ (molecular weight: 2.60×10^6) were formed by 104 molecules.[9,10] $P_{296}D_1$ (molecular weight: 2.20×10^7) formed vesicles (hydrodynamic diameter: 230 nm, TEM diameter: 240 nm) consisting of 241 molecules.[11] The aggregation number was calculated by dividing the molecular weight of the aggregate by the molecular weight of a single polymer chain.[9,11]

2.2. Preparation of Polymer-FGA, Polymer/DOX, and Polymer-FGA/DOX

FGA was chemically bound on $P_{71}D_3$ and $P_{296}D_1$ by an amidation reaction[12] between a free carboxylate group at a terminal of hydrophilic block of polymers and an amine group of FGA to obtain $P_{71}D_3$-FGA and $P_{296}D_1$-FGA, respectively. A suspension of $P_{71}D_3$ in water or $P_{296}D_1$ in methanol (0.1 mg mL^{-1}) was mixed with a freshly prepared aqueous solutions of EDC and NHS, and the mixture was allowed to stand for 1 h to produce NHS-activated carboxylate. Then, FGA (1 μg mL^{-1}) was added to the mixture to conjugate to the block copolymer through the formation of an amide bond. Unbound FGA was removed by ultracentrifugation at 9300 × g for 1 h. The obtained residue was rinsed three times with water or methanol. The amount of FGA conjugated on both $P_{71}D_3$ micelles and $P_{296}D_1$ vesicles was determined by estimating the FGA fluorescence emission intensity (area under the curve, AUC) from 500 to 540 nm following excitation at 488 nm. 100 mL of $P_{71}D_3$/FGA and $P_{296}D_1$/FGA were added to the 96-well black plate (Corning, NY, USA) and the emission intensity was measured using a SpectraMax M3 multimode microplate reader (Molecular Devices, Sunnyvale, CA, USA). The AUC was calculated using ImageJ 1.49 (NIH, Bethesda, MD, USA). The emission intensity (AUC) for $P_{71}D_3$-FGA was slightly higher than that of $P_{296}D_1$-FGA, with a difference of 9%. This suggests that almost similar amount of FGA was conjugated to both amphiphilic polymers.

$P_{71}D_3$ or $P_{71}D_3$-FGA (0.5 mg) and DOX (0.1 mg) were dissolved in water (5 mL). An aqueous solution of DOX (2 mg mL^{-1}) was added to a methanolic solution of $P_{296}D_1$ or $P_{296}D_1$-FGA (0.5 mg mL^{-1}). Methanol was then evaporated under reduced pressure, and the residue was dissolved in water (5 mL). All polymer solutions were allowed to stand overnight at room temperature to achieve complete dissolution. The aqueous solutions (5 mL) were dialyzed against water using a regenerated cellulose dialysis tube (MWCO of 6000–8000 g mol^{-1}) over 32 h at room temperature until all free DOX was removed.

2.3. Loading and Release of DOX

The amount of DOX entrapped in the polymeric nanocarriers was determined from the absorbance of a 232 nm band based on a calibration curve with known concentrations of DOX up to 150 μg mL^{-1} in water in accordance with the procedure previously reported.[13] The determined amount of unbound DOX in the dialyzed outer solution was subtracted from the initial amount of DOX to calculate the amount of loaded DOX.

The release of DOX from polymeric nanocarriers was studied in phosphate buffer saline (PBS) at two different pH values (pH 7.4 and 5.5). The nanocarriers were suspended in 1 mL of PBS to obtain a concentration of 30 μg mL^{-1} of DOX equivalent. The tubes were sealed and incubated at 37 °C at 100 rpm in an orbital shaker (ZHWY 103D, Labwit, Shanghai, China). At predetermined time intervals of 0.25, 0.5, 1, 2, 4, 6, 8, 24, and 48 h, the samples were centrifuged at 9300 × g for 10 min and the supernatants containing the released DOX were collected and replaced with fresh buffer. The amount of DOX released was determined using a spectrophotometer as described above.[14,15]

2.4. In Vitro Cytotoxicity of $P_{71}D_3$/DOX Micelles and $P_{296}D_1$/DOX Vesicles

Aqueous stock solutions (100 μg mL^{-1} polymer) of $P_{71}D_3$, $P_{296}D_1$, $P_{71}D_3$/DOX (95 μg mL^{-1} DOX equivalent polymer), and $P2_{96}D_1$/DOX (40 μg mL^{-1} DOX equivalent polymer) nanocarriers were prepared. The MDA-MB-231 cell line was grown and maintained in Dulbecco's modified Eagle's medium (DMEM) supplemented with 10% fetal bovine serum (FBS) and 1% penicillin-streptomycin at 37 °C in a 5% CO_2 humidified chamber. MDA-MB-231 cells were seeded into 96-well plates at 5000 cells per well and were incubated overnight to allow cells to adhere before polymer samples were introduced. Polymer samples were diluted in culture medium and added to the cells to give final concentrations ranging from 0.03 to 10 μg mL^{-1} DOX equivalent. The cells were then incubated for 24 h at 37 °C in 5% CO_2 before cell viability was assessed using the 3-(4,5-dimethylthiazol-2-yl)-2,5-diphenyl tetrazolium bromide (MTT) assay. Briefly, 10 μL of MTT (5 mg mL^{-1} in PBS) was added to each well and incubated for 3 h. The supernatant was removed, and 100 μL of dimethylsulfoxide was added to dissolve the purple formazan crystal. The optical density of each well was measured at 570 nm using a microplate reader. The viability of the cells in response to the treatment of polymer samples was calculated as a percentage (%) of cell viability = (OD treated/OD control) × 100. Cell viability in the presence of a solvent control (PBS) was determined concurrently.

2.5. Cellular Uptake of Polymer/DOX by Flow Cytometry and Polymer-FGA, Polymer/DOX, and Polymer-FGA/DOX by Confocal Microscopy

The uptake of $P_{71}D_3$/DOX, $P_{296}D_1$/DOX, and free DOX by MDA-MB-231 cells was investigated using flow cytometry. The cells (1.5×10^5 cells per well), which were seeded in 12-well culture plates and incubated for 24 h at 37 °C in a 5% CO_2 humidified chamber, were treated with $P_{71}D_3$/DOX, $P_{296}D_1$/DOX, or free DOX (1 μg mL^{-1} DOX equivalent) at predetermined time intervals (1, 2, and 5 h) or different concentrations (0, 0.625, 1.25, 2.5, 5, and 10 μg mL^{-1}) with 2 h incubations. The treated cells were washed two times with cold PBS, trypsinized, transferred to tubes, and centrifuged. The cells were resuspended in 0.5 mL of PBS containing 0.5% FBS for immediate flow cytometric analysis on a BD FACS Canto II flow cytometer (Becton Dickinson, San Jose, CA, USA) equipped with a 488 nm argon laser and a 670 nm long pass filter to detect the fluorescence emitted by the DOX taken up by the cells. Data from 10 000 cells were collected and analyzed using FACS DIVA analysis software (Becton Dickinson).

The procedure for confocal microscopy was as follows: MDA-MB-231 cells (2×10^5 cells per well) in complete DMEM culture medium were seeded on glass coverslips (22 × 22 mm), placed in 6-well plates and incubated for 24 h at 37 °C in a 5% CO_2 humidified chamber. The cells were treated with 10 μg mL^{-1} polymer of $P_{71}D_3$-FGA, $P_{296}D_1$-FGA, $P_{71}D_3$/DOX (1 μg mL^{-1} DOX equivalent), $P_{296}D_1$/DOX (1 μg mL^{-1} DOX equivalent), $P_{71}D_3$-FGA/DOX (1 μg mL^{-1} DOX equivalent), or $P_{296}D_1$-FGA/DOX (1 μg mL^{-1} DOX equivalent) for 3 h at 37 °C. The cells were fixed with 4% paraformaldehyde on a glass coverslip for 10 min at 37 °C and then rinsed twice with PBS. Fixed cells on glass coverslips were mounted on glass slides with mounting medium containing 4′,6-diamidino-2-phenylindole (DAPI) (Slow Fade Gold Antifade Mount, Life Technologies Inc., Carlsbad, CA, USA). Cellular uptake of the nanoparticles was observed with a confocal laser scanning microscope using a 63× oil immersion objective (Leica TCS SP5 II, Leica Microsystem, Wetzlar, Mannheim, Germany). The DAPI dye was excited using a 405 nm diode laser and had its emission detected between 414 and 481 nm on the photomultiplier tube (PMT). Both FGA labeled nanoparticles and DOX were excited using a 488 nm argon laser and had their emissions detected between 494–542 nm for FGA and 590–720 nm for DOX on the PMT detector. All scans were performed in an independent sequential mode to avoid spectral overlap during acquisitions. Images were captured using the Leica LAS-AF image capture software. All the data used for quantitative comparisons of cell fluorescence intensities were acquired under identical conditions with constant gain and offset. The fluorescence intensity of DOX was analyzed using Leica Application Suite-X (LAS-X) software by selecting the Regions of Interest (ROI) to determine the sum of the intensity of each pixel in a cell (gray value). The integrated density of fluorescence (IDF) was then calculated from the mean gray value obtained from a total of 10 cells multiplied by the ROI (mean gray value × ROI).[16]

Sequential optical sections (Z-stacks) from the apical-to-basal surfaces of the cell were acquired, initiated ≈1 μm below the above apical of the cells, and optical slices were collected at 1 μm steps through their basal surface using a 63× oil immersion objective. These wide-field images were subjected to deconvolution using LAS-X software.

To assess the effect of temperature on the uptake of nanoparticles, the flow cytometric and confocal microscopic cellular uptake studies were repeated based on the procedures described previously, except the cells were treated with nanocarriers for either 2 h (flow cytometry) or 3 h (confocal microscopy) at 4 and 37 °C, respectively.

2.6. Intracellular Colocalization of Polymer-FGA, and Polymer/DOX Nanocarriers

The intracellular localization of the $P_{71}D_3$/DOX, $P_{296}D_1$/DOX, and free DOX was analyzed by confocal microscopy using dual staining techniques as previously reported.[17] Briefly, MDA-MB-231 cells grown on coverslips in 6-well plates were incubated with test samples for 3 h, as described in the confocal cellular uptake studies above. The cells were then rinsed twice with PBS to remove free DOX or free nanocarriers. Subsequently, the cells were stained with an organelle-specific fluorescence probe. The mitochondria, endoplasmic reticulum, and lysosomes were stained with 100×10^{-9} M MitoTracker Green, 100×10^{-9} M ER-Tracker Blue-White DPX, and 100×10^{-9} M LysoTracker Blue, respectively. Meanwhile, the colocalization of $P_{71}D_3$-FGA and $P_{296}D_1$-FGA nanocarriers was studied using FGA fluorescence along with 100×10^{-9} M MitoTracker Red, 100×10^{-9} M ER-Tracker Blue-White DPX, and 100×10^{-9} M LysoTracker Blue.

Cells were incubated with each stain for ≈30 min at room temperature. Following incubation, the cells were rinsed with PBS to remove free dye, and the stained cells were observed using a confocal laser scanning microscope configured with a 63× oil objective (Leica TCS SP5 II). The LysoTracker and ER-Tracker were excited using a 405 diode laser line where the PMT setting for

the emission signal was 413–481 nm. Both MitoTracker dyes were excited using a multi-line Argon laser 488 line (the PMT settings for the emission detector were 494–524 nm for MitoTracker Green and 497–573 nm for MitoTracker Red). All scans were performed with an independent sequential mode; hence, there was no spectral overlap in the acquisition. The intracellular localization of the test samples was determined by comparing the fluorescence topographic profile of each organelle probe generated from a longitudinal transcellular axis.

3. Results and Discussion

3.1. Characterization of $P_{71}D_3$/DOX Micelles and $P_{296}D_1$/DOX Vesicles

The amphiphilic diblock copolymers, $P_{71}D_3$ and $P_{296}D_1$ (see Scheme 1), which consisted of a hydrophilic linear chain block and a hydrophobic block with a pendant dendron side chain, are self-assembled into micelles and vesicles, respectively.[9,11] They can be expected to encapsulate small molecules in their self-assemblies because these polymer aggregates possess a large void volume for trapping small molecules. To evaluate their potential as carriers in drug delivery systems, the anticancer drug DOX was loaded into the aggregates. The loading of DOX in weight per unit weight of the diblock copolymer in both $P_{71}D_3$ micelles and $P_{296}D_1$ vesicles was almost linear for the initial increase in the DOX concentration in the incubation solution, but was nearly doubled for the $P_{71}D_3$ micelles compared with the $P_{296}D_1$ vesicles (Figure 1A). Nevertheless, the loading of micelles gradually converged with a constant value of 2.3 g g^{-1} (polymer) (Figure 1A).

Figure 1B plots the loading number of DOX per polymer aggregate, which was recalculated from the loading amount using adequate aggregate parameters,[9,11] as a function of the DOX concentration. The number of DOX molecules entrapped per aggregate was similar for both aggregates up to a 0.4 mg mL^{-1} DOX concentration. However, for the $P_{71}D_3$ micelles, the loading number was saturated at 104 for 0.5 mg mL^{-1} of DOX, which was the same as the aggregation number (104) of micelles, indicating that the encapsulation maximum is one DOX per one polymer chain. This number was larger than the uptake of pyrene (23 molecules) and was comparable with 1,1-diphenyl-2-picrylhydrazyl radicals (104 molecules).[10b] Conversely, the encapsulation number for the P_{296}D1 vesicle increased linearly to 136 for the 0.52 mg mL^{-1} DOX concentration. This indicates that a large number of DOX molecules can be entrapped within the interior water pool of vesicles.

The absorption band of DOX in P_{296}D1 vesicles was the same as that of free DOX in water at 490 nm (Figure 2A), indicating the entrapping of DOX in the interior water pool of vesicles. However, the band in $P_{71}D_3$ micelles was

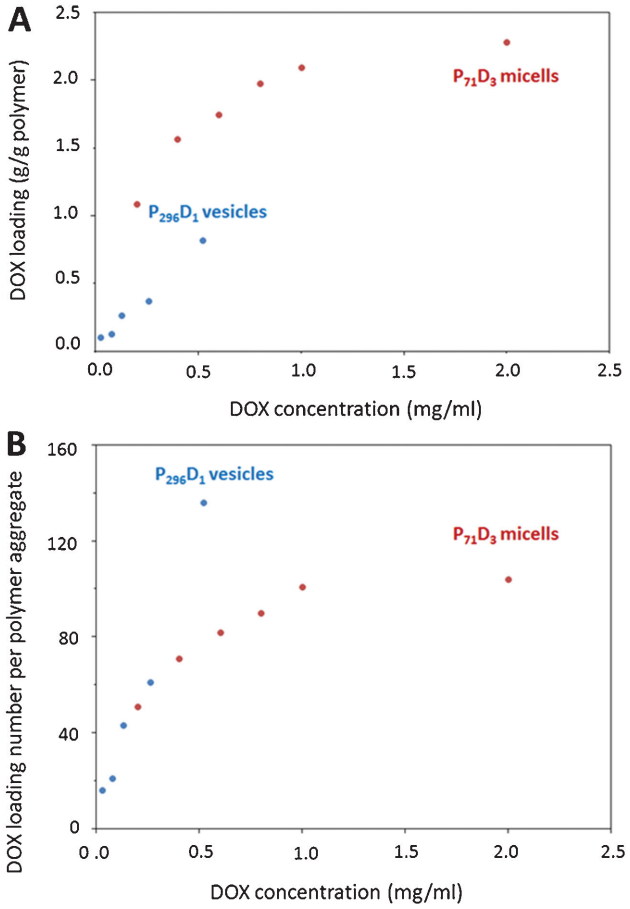

Figure 1. DOX loading in $P_{71}D_3$/DOX micelles and $P_{296}D_1$/DOX vesicles as a function of DOX concentration. A) Weight per polymer weight and B) Number per polymer aggregate.

redshifted to 510 nm (Figure 2B); this variation suggests the environmental change of DOX from a water medium to the hydrophobic interior of a polymer micelle, as presented in Scheme 1.

3.2. In Vitro DOX Release from $P_{71}D_3$/DOX Micelles and $P_{296}D_1$/DOX Vesicles

The time-dependent release of DOX from polymer aggregates was compared in Figure 3A. The release from both nanocarriers/DOX was rapid initially but almost reached a steady state at 10 h, although gradual release continued even up to 48 h. The percentage of DOX released from $P_{71}D_3$/DOX micelles was lower than that released from $P_{296}D_1$/DOX vesicles. A higher percentage of DOX was released from $P_{71}D_3$/DOX micelles at a pH of 5.5 compared with a pH of 7.4. Meanwhile, the $P_{296}D_1$/DOX vesicles had similar percentages of released DOX at both a pH of 5.5 and a pH of 7.4.

Figure 3B shows the percentage of released DOX from $P_{296}D_1$/DOX vesicles at different DOX concentrations. The percentage released decreased with increasing DOX con-

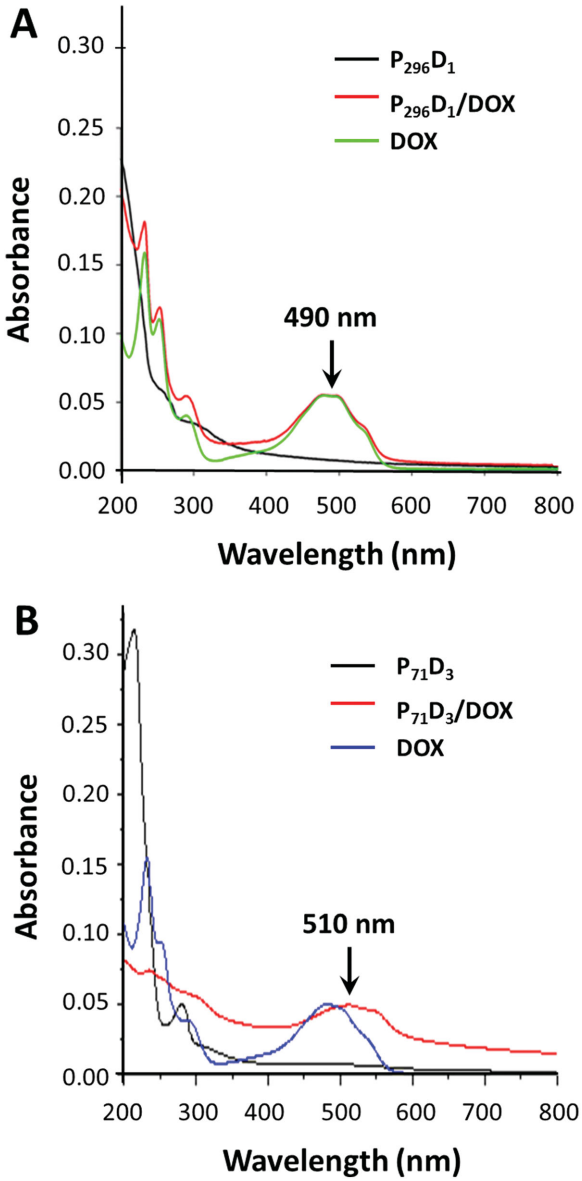

Figure 2. Comparison of UV–vis absorption spectra. A) $P_{296}D_1$, DOX, and $P_{296}D_1$/DOX, and B) $P_{71}D_3$, DOX, and $P_{71}D_3$/DOX.

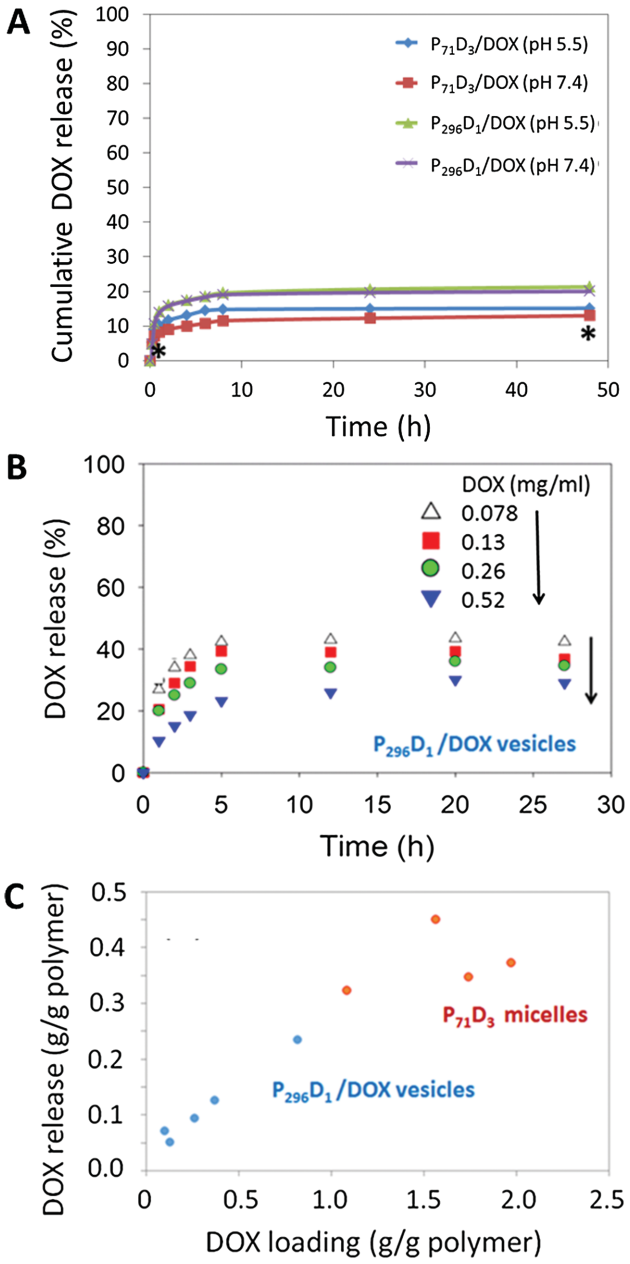

Figure 3. A) Percentage of DOX released time course from $P_{71}D_3$/DOX micelles and $P_{296}D_1$/DOX vesicles in phosphate buffer saline (PBS) at pH 5.5 and 7.4. Data are expressed as the mean ± SD ($n = 3$). *$p < 0.05$ using Student's t-test for $P_{71}D_3$/DOX at pH 5.5 and pH 7.4. B) Percentage of DOX released time course from $P_{296}D_1$/DOX vesicles at different DOX concentrations. C) DOX released per weight of polymer from $P_{71}D_3$/DOX micelles and $P_{296}D_1$/DOX vesicles against DOX loading.

centrations. However, when analyzed according to the loading amount in g g^{-1} polymer, the DOX release profile from the two different diblock copolymer structures behaved differently depending on the different loading amounts. That is, the amount of DOX released increased up to 0.24 g g^{-1} polymer for $P_{296}D_1$/DOX vesicles but was almost constant at ≈0.37 g g^{-1} polymer for $P_{71}D_3$/DOX micelles (Figure 3C).

The release conditions in this study simulated the drug release environment of the human body, assuming that DOX is injected intravenously into an adult at its therapeutic dosage of 60 mg m^{-2},[18] and the adult plasma volume is 55% of 5 L of blood.[19] Our results suggested that the percentage of DOX released from the $P_{71}D_3$ micelles after an intravenous injection was minimal over 48 h at ≈15%–20%. Moreover, $P_{71}D_3$/DOX micelles are likely to enhance DOX release in the acidic tumor interstitium or within the lysosomes after cellular uptake, which was shown by the DOX release profile at a pH of 5.5.[20] This

difference is of statistical significance at certain time point indicated with the (*) sign as presented in Figure 3A.

Since the hydrophilic blocks of $P_{71}D_3$ consist of side chain with a strong acid group ($-SO_3^{-1}$), equivalent amounts of counterion (Na^+) are coexisting in the hydrophilic shell of $P_{71}D_3$ micelles at neutral pH (≈7). However, when the ionic strength increases in acidic conditions like pH 5.5, excess ions are condensed in the hydrophilic shell of micelles. The resultant osmotic pressure and the electrostatic repulsion cause the shell volume to increase and thus, the loaded DOX can be released easier than those at the neutral condition. This phenomenon of swelling in response to changes in the ionic strength and pH[21] is a characteristic of polymers and their aggregates, which is different from the behavior of small molecules. This characteristic of differential release in $P_{71}D_3$/DOX micelles is desirable because DOX leakage is minimized in the systemic circulation but is enhanced in tumor localization.

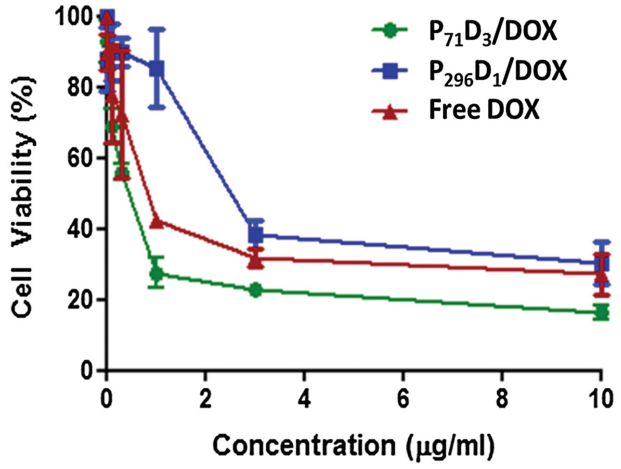

Figure 4. The effect of $P_{71}D_3$/DOX micelles, $P_{296}D_1$/DOX vesicles, and free DOX on the cell viability of MDA-MB-231 cells at 37 °C and 24 h incubation. Data are represented as the mean ± SD ($n = 3$).

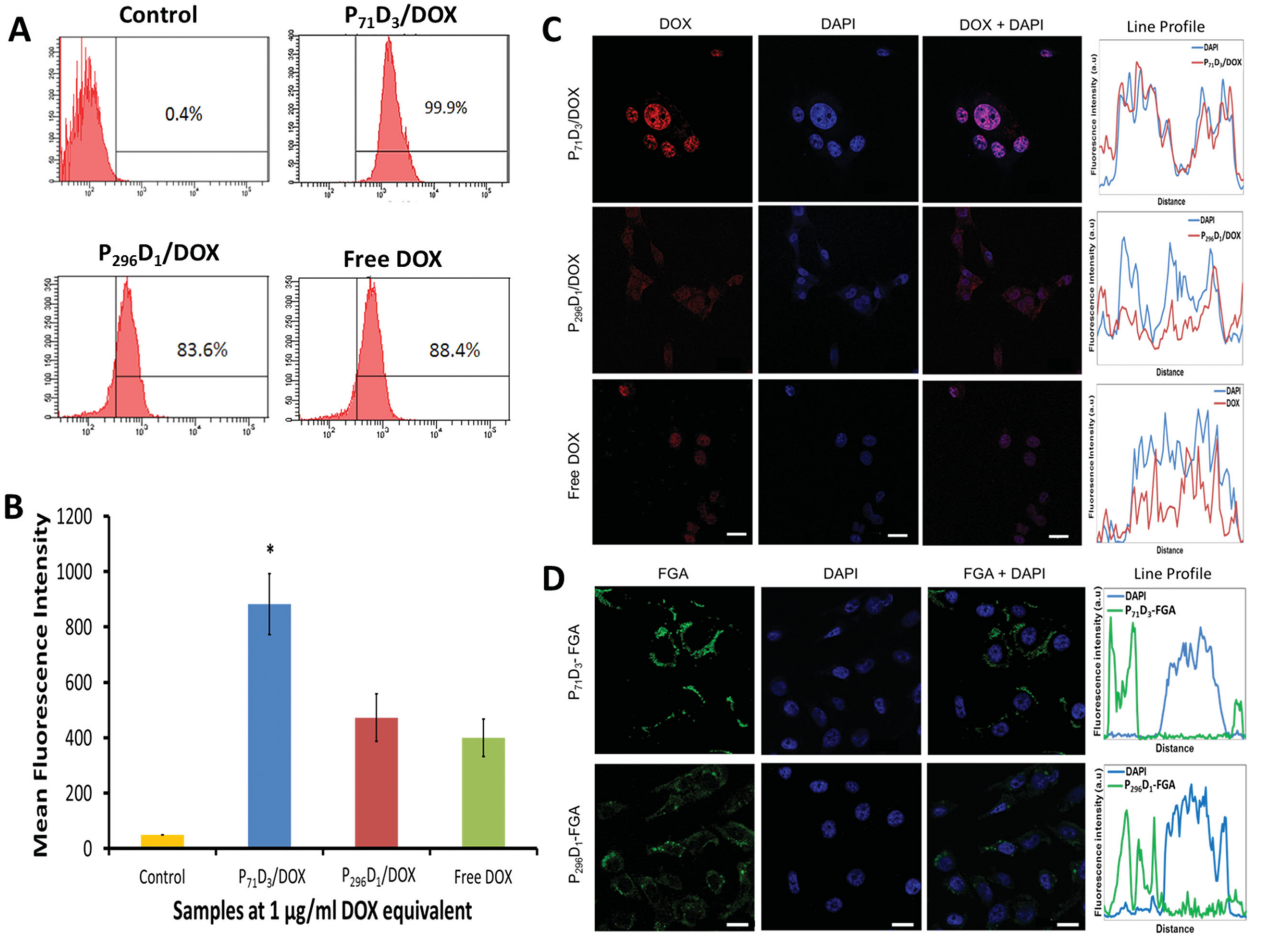

Figure 5. Cellular uptake of $P_{71}D_3$/DOX micelles, $P_{296}D_1$/DOX vesicles, and free DOX by MDA-MB-231 cancer cells using flow cytometry and confocal microscopy. A) Percentage of cellular uptake for nanocarriers/DOX and free DOX on cells. B) Mean fluorescence intensity of polymer/DOX and free DOX in cells. Data are expressed as the mean ± SD ($n = 3$). *$p < 0.05$ using one-way ANOVA. C) Confocal microscopic images and line profiles of polymer/DOX and free DOX on DAPI-labeled cells. Scale bar: 20 μm. D) Confocal microscopic images and line profiles of FGA-treated polymers on DAPI-labeled cells. Scale bar: 20 μm.

The difference in drug loading/release behavior between the two polymer nanocarriers may be due to the shape of nanocarriers. Since the hydrophilic block in $P_{71}D_3$ has a maximum length of ≈12.3 nm, polymer micelles with a diameter of 70.5 nm can possess a core volume with a diameter of 46 nm (Scheme 1). This core size is large enough to encapsulate many units of DOX molecules such as the calculated 104 units in this study. Although a DOX molecule has hydrophilic functional (amine and phenol) groups and is water soluble, it is fundamentally amphiphilic because DOX consists of an aromatic backbone. Therefore, many DOX molecules may be encapsulated in the micellar core, whereas some molecules will be close to the core/shell border, resulting in an easier release. Since the $P_{296}D_1$ vesicle with a 240 nm diameter has a wall vesicle thickness of ≈50 nm (Scheme 1), the hydrophobic core layer in the vesicle bilayer is most likely not thick enough to encapsulate DOX molecules. Therefore, the loading of DOX was assumed to occur only at the internal water pool in the vesicles; these DOX molecules permeated out into the surrounding by passing through the thin hydrophobic core layer of the vesicle membrane.

3.3. In Vitro Cytotoxicity of $P_{71}D_3$/DOX Micelles and $P_{296}D_1$/DOX Vesicles

The MDA-MB-231 cancer cell viability following treatment was determined 24 h later using the MTT assay (Figure 4). The $P_{71}D_3$/DOX micelles exhibited enhanced cytotoxicity, with an IC_{50} of 0.62×10^{-6} M (0.34 μg mL^{-1}) DOX equivalent compared with free DOX ($IC_{50} = 1.46 \times 10^{-6}$ M or 0.79 μg mL^{-1}) and $P_{296}D_1$/DOX ($IC_{50} = 4.45 \times 10^{-6}$ M or 2.42 μg mL^{-1}) treatments under identical conditions. Our IC_{50} value for free DOX was within the range of IC_{50} found in the literature, from 0.025×10^{-6} to 2.7×10^{-6} M, for MDA-MB-231 cells.[22] This confirms that the $P_{71}D_3$/DOX micelles have a higher potency compared with free DOX whereas $P_{296}D_1$/DOX vesicles have the least potency.

As a control, cells treated with up to 10 μg mL^{-1} $P_{71}D_3$ micelles or $P_{296}D_1$ vesicles showed no reduction in cell viability (data not shown). This implies that the observed cytotoxicity of $P_{71}D_3$/DOX and $P_{296}D_1$/DOX is due to the DOX in the $P_{71}D_3$ micelles or $P_{296}D_3$ vesicles. The higher cytotoxic potency of the $P_{71}D_3$/DOX micelles corresponds to their higher cellular uptake compared with free DOX and $P_{296}D_1$/DOX vesicles (refer to Section 3.4).

3.4. Cellular Uptake of $P_{71}D_3$/DOX Micelles and $P_{296}D_1$/DOX Vesicles

Cellular uptake of the $P_{71}D_3$/DOX micelles, $P_{296}D_1$/DOX vesicles, and free DOX by MDA-MB-231 cancer cells was quantified with flow cytometry based on the fluorescence of DOX. The $P_{71}D_3$/DOX micelles exhibited the highest cellular uptake of 100% after incubation for 2 h compared with the $P_{296}D_1$/DOX vesicles (84%) and free DOX (88%) (Figure 5A). Incidentally, the mean fluorescence intensities of the MDA-MB-231 cells treated with $P_{71}D_3$/DOX micelles were approximately two times higher than the cells treated with an equivalent dose of $P_{296}D_1$/DOX vesicles and free DOX (Figure 5B, $p < 0.05$, one-way ANOVA with Bonferroni post-hoc test).

The cellular uptake of DOX in free micellar or vesicular forms at an equivalent dose was also evaluated with confocal microscopy. The red fluorescence of DOX observed in the MDA-MB-231 cells treated with $P_{71}D_3$/DOX micelles was brighter than in the cells treated with $P_{296}D_1$/DOX vesicles and free DOX (Figure 5C). Similar observations on the green fluorescence intensity were also found in the MDA-MB-231 cells treated with $P_{71}D_3$-FGA micelles, $P_{296}D_1$-FGA vesicles (Figure 5D), which have the similar amount of FGA conjugated to both amphiphilic polymers. The results from cellular uptake suggested an enhanced accumulation of $P_{71}D_3$/DOX micelles in the cells. The decreasing order of cellular uptake was as follows: $P_{71}D_3$/DOX > DOX > $P_{296}D_1$/DOX and was in agreement with that of the corresponding cytotoxicity potency.

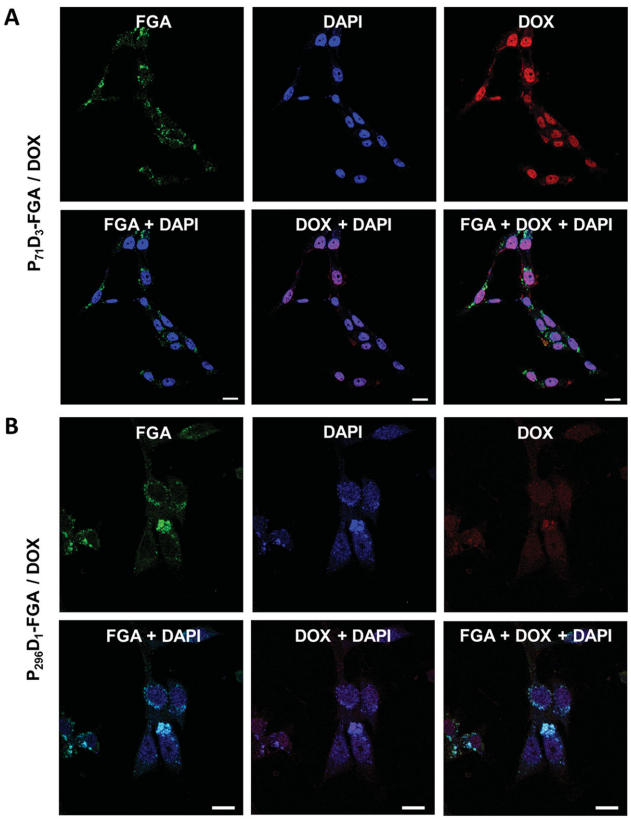

Figure 6. Confocal microscopic images of MDA-MB-231 cells treated with polymer-FGA/DOX. DAPI was used as a counterstain to visualize the nuclei. A) $P_{71}D_3$ micelles and B) $P_{296}D_1$ vesicles.

In the cells treated with $P_{71}D_3$/DOX micelles, high intensities of red fluorescence were found in the nuclear compartment, but not in the cytoplasm (Figure 5C). This suggested that DOX is released from the $P_{71}D_3$ micelles in the acidic environment of the tumor lysosomes upon cellular uptake, which allowed DOX into diffuse to the nucleus, as discussed in Section 3.2. This is supported by the high green fluorescence intensity observed in the cytoplasm, but not the nuclei of the $P_{71}D_3$-FGA treated cells (Figure 5D).

In the cells treated with $P_{296}D_1$/DOX vesicles, red DOX fluorescence intensity was found to be lower in the nuclei, with some intensity was also noted in the cytoplasm (Figure 5C). The localization of the green $P_{296}D_1$-FGA fluorescence in the cytoplasm with minimal overlapping with the DAPI in nuclei of the treated cells suggested that the $P_{296}D_1$/DOX vesicles within the cells remained mainly in the cytoplasm and only some had entered the nuclei (Figure 5D).

Previous observations were further confirmed and more apparent when cells were treated with DOX-loaded and fluorescence-labeled $P_{71}D_3$-FGA/DOX micelles and $P_{296}D_1$-FGA/DOX vesicles (Figure 6), where the cellular accumulation of DOX-entrapped carriers and the cellular localization of DOX were evaluated concurrently. The uptake of the $P_{71}D_3$-FGA/DOX micelles was again much greater than the uptake of the $P_{296}D_1$-FGA/DOX vesicles. The level of DOX localized in the nuclei in the $P_{71}D_3$-FGA/DOX-treated cells was significantly higher than that localized in the nuclei of the $P_{296}D_1$-FGA/DOX-treated cells. These results agreed with the cytotoxicity data, where the $P_{71}D_3$/DOX micelles had the highest cellular uptake and localization of DOX in the nuclei, as well as the highest potency, followed by free DOX and $P_{296}D_1$/DOX vesicles (Figure 4). Nuclear uptake of DOX is crucial to enable DOX to interact with DNA through intercalation, which leads to the disruption of topoisomerase-II-mediated DNA repair. This prevents the DNA double helix from being resealed after unwinding for replication, resulting in DNA damage and cell death.[23]

To investigate the extent of intracellular drug accumulation with the DOX concentrations used in cell viability tests, the cellular uptake of $P_{71}D_3$/DOX micelles, $P_{296}D_1$/DOX vesicles, or free DOX in MDA-MB-231 cells

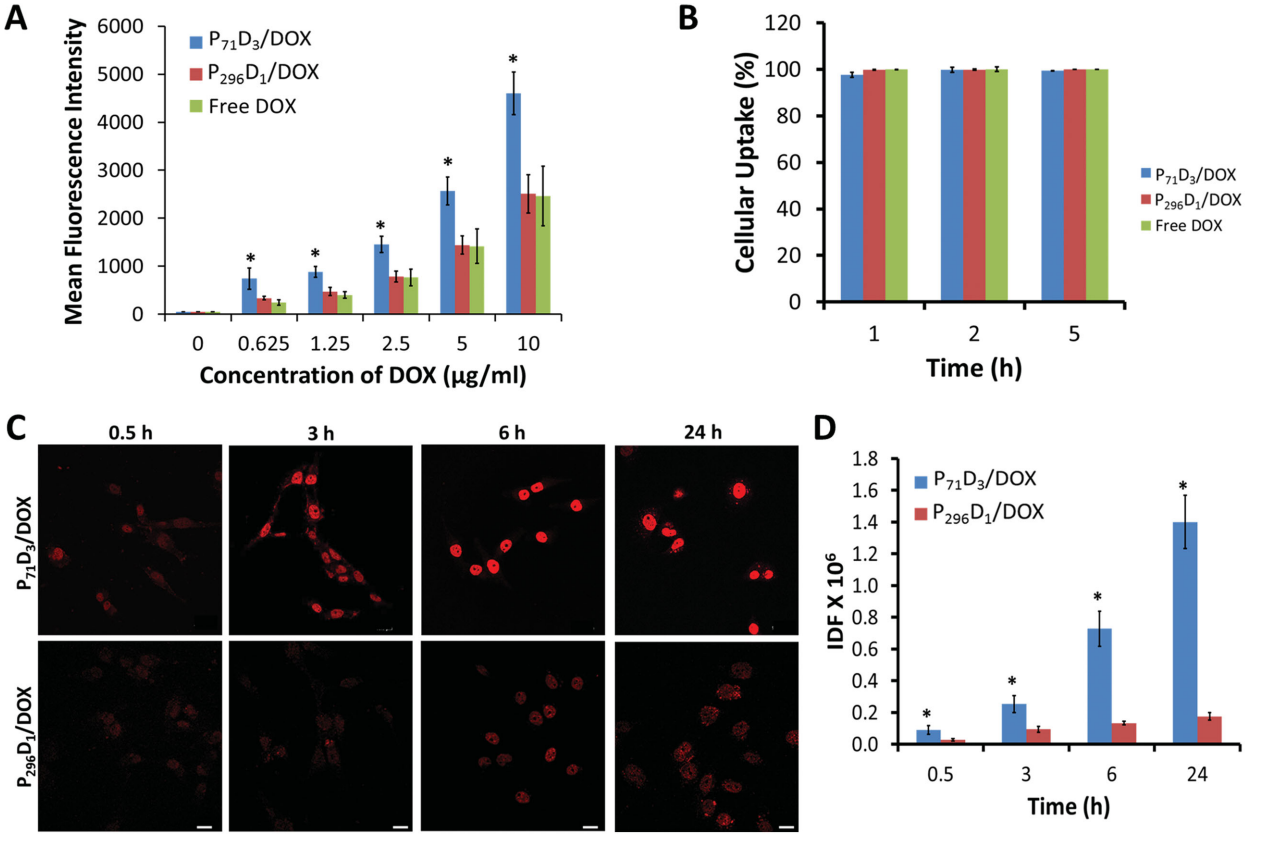

Figure 7. Cellular uptake of $P_{71}D_3$/DOX micelles, $P_{296}D_1$/DOX vesicles, and free DOX in MDA-MB-231 cells. A) DOX concentration dependence of cellular uptake from fluorescence intensity. Data are expressed as the mean ± SD ($n = 3$). *$p < 0.05$ using one-way ANOVA. B) Time dependence of cellular uptake from percentage of cellular uptake. Data are expressed as the mean ± SD ($n = 3$). C) Time dependence of cellular uptake from confocal microscopy. Scale bar: 20 μm. D) Time dependence of cellular uptake from fluorescence intensity. Data are expressed as the mean ± SD ($n = 3$). *$p < 0.05$ using independent *t*-test.

were quantified using flow cytometry, after 2 h of incubation with DOX concentrations ranging from 0–10 μg mL^{-1}. The mean fluorescence intensities of DOX were used to estimate the level of $P_{71}D_3$/DOX micelles, $P_{296}D_1$/DOX vesicles, or free DOX taken up by the cells (Figure 7A). Cellular uptake increased in a concentration-dependent manner in which the uptake amount was in the following order: $P_{296}D_1$/DOX vesicles ≈ free DOX < $P_{71}D_3$/DOX micelles, and the uptake of $P_{71}D_3$/DOX was approximately two times higher than the uptake of free DOX and $P_{296}D_1$/DOX ($p < 0.05$, one-way ANOVA with Bonferroni post-hoc test). Cellular uptake of $P_{71}D_3$/DOX micelles, $P_{296}D_1$/DOX vesicles, or free DOX (1 μg mL^{-1} DOX equivalent) in MDA-MB-231 cells was also quantified at different time intervals of 1, 2, and 5 h. The $P_{71}D_3$/DOX micelles, $P_{296}D_1$/DOX vesicles, and free DOX were taken up by 100% of the treated cells, beginning at 1 h after incubation (Figure 7B).

The cellular uptake of the $P_{71}D_3$/DOX micelles and $P_{296}D_1$/DOX vesicles was also investigated using confocal microscopy based on the red fluorescence of DOX at different time intervals of 0.5, 3, 6, and 24 h in the MDA-MB-231 cancer cells (Figure 7C). Based on the DOX IDF derived from confocal microscopy, the cellular uptake of $P_{71}D_3$/DOX increased in a time-dependent manner whereas $P_{296}D_1$/DOX showed a much lower increase in uptake (Figure 7D, $p < 0.05$ using independent t-test). These results indicated that the delivery of DOX using $P_{71}D_3$ micelles efficiently increased the cellular DOX concentration in the MDA-MB-231 cells compared with the $P_{296}D_1$ vesicles.

3.5. Cellular Uptake via Energy-Dependent Mechanism

The MDA-MD-231 cells were treated with $P_{71}D_3$/DOX micelles and $P_{296}D_1$/DOX vesicles to determine the cellular uptake mechanism, intracellular localization, and accumulation. Endocytosis is one of the main cellular uptake mechanisms for various extracellular materials and nanocarriers. Almost all endocytic pathways are energy-dependent processes that can be inhibited at low temperatures, for example, at 4 °C.[24] Figure 8A shows that the incubation of the MDA-MB-231 cells with $P_{71}D_3$/DOX micelles and $P_{296}D_1$/DOX vesicles at 4 °C for 2 h caused a 90%–92% decrease in DOX uptake compared with the cells incubated at 37 °C, as measured by flow cytometry.

Temperature-dependent localization of the $P_{71}D_3$/DOX micelles and $P_{296}D_1$/DOX vesicles in MDA-MB-231 cells was also studied using confocal microscopy. The uptake of $P_{71}D_3$-FGA/DOX and $P_{296}D_1$-FGA/DOX, which was indicated by the green fluorescence of FGA-labeled nanocarriers and the red fluorescence of DOX, was significantly reduced when the treated cells were incubated at 4 °C (Figure 8B). This indicates that the internalization of $P_{71}D_3$/DOX micelles and $P_{296}D_1$/DOX vesicles into MDA-MB-231 cells most likely occurred via energy-dependent processes, which contrasts the diffusion-based translocation of free DOX.[25]

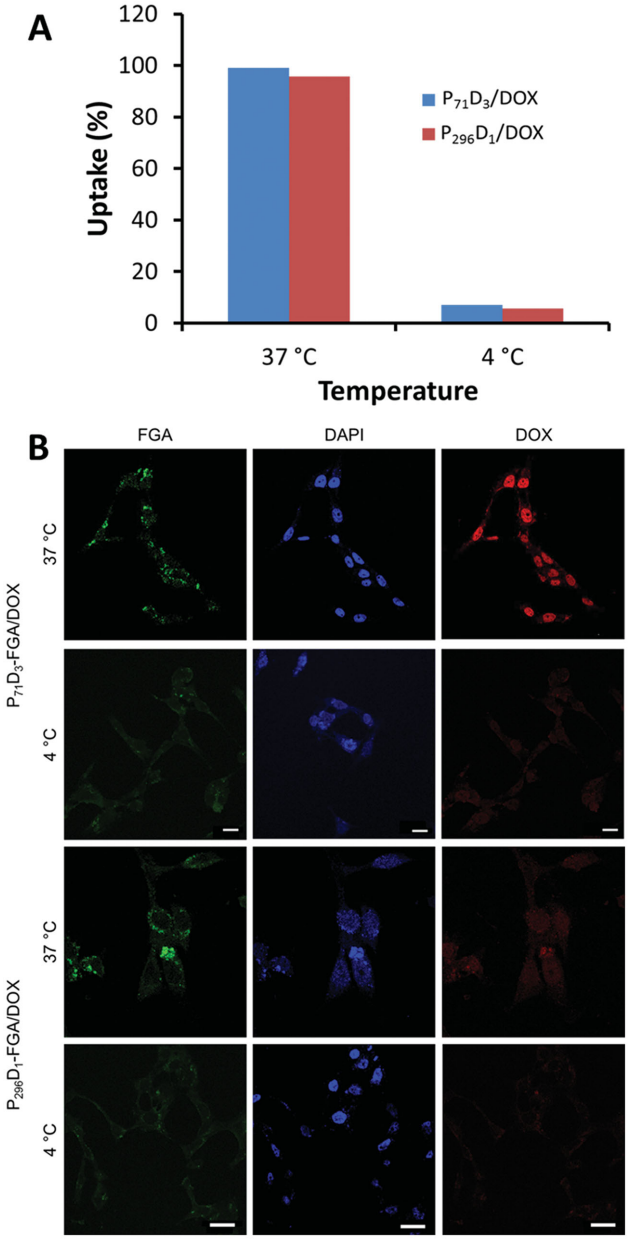

Figure 8. Temperature dependence of cellular uptake for $P_{71}D_3$/DOX micelles and $P_{296}D_1$/DOX vesicles on MDA-MB-231 cells. A) Percentage of cellular uptake for nanocarriers and B) confocal microscopy of FGA-labeled nanocarriers. Scale bar: 20 μm.

3.6. Intracellular Localization of $P_{71}D_3$/DOX Micelles and $P_{296}D_1$/DOX Vesicles

To determine the intracellular localization of the $P_{71}D_3$/DOX micelles and $P_{296}D_1$/DOX vesicles, $P_{71}D_3$-FGA and $P_{296}D_1$-FGA (green fluorescence) were used together with LysoTracker (blue), ER-Tracker (blue), and MitoTracker

(red) as the markers for the lysosomes, endoplasmic reticulum, and mitochondria, respectively. Figure 9A,B shows high colocalization of green fluorescence with LysoTracker, suggesting that both the $P_{71}D_3$ micelles and the $P_{296}D_1$ vesicles were internalized into the MDA-MB-231 cells by endocytosis and localized in the lysosomes, which is the last compartment in the endocytic pathway. Both $P_{71}D_3$-FGA and $P_{296}D_1$-FGA also showed localization in mitochondria and minimal accumulation in the endoplasmic reticulum.

To identify the intracellular distribution of DOX (red fluorescence) delivered by $P_{71}D_3$/DOX micelles and $P_{296}D_1$/DOX vesicles, colocalization assays were again performed with organelle-specific fluorescence probes. The DOX from $P_{71}D_3$/DOX and $P_{296}D_1$/DOX was only partially colocalized with the LysoTracker (Figure 10A,B) although their FGA-labeled carriers showed a significant colocalization signal with LysoTracker (Figure 9). This suggested that the DOX may escape from the lysosomes, translocate, and accumulate in the nuclei, as shown in Figure 5C. Our results are in agreement with those of Wei et al.[26] and Cui et al.,[27] who suggested that the DOX loaded in the amphiphilic-dendrimer nanomicelles and amphiphilic poly(ethylene glycol) derivative micelles could successfully escape from the lysosomes into the cytoplasm of both the breast cancer MCF-7R cells and cervical cancer HeLa cells. Finally, the released DOX could effectively enter the nuclei.

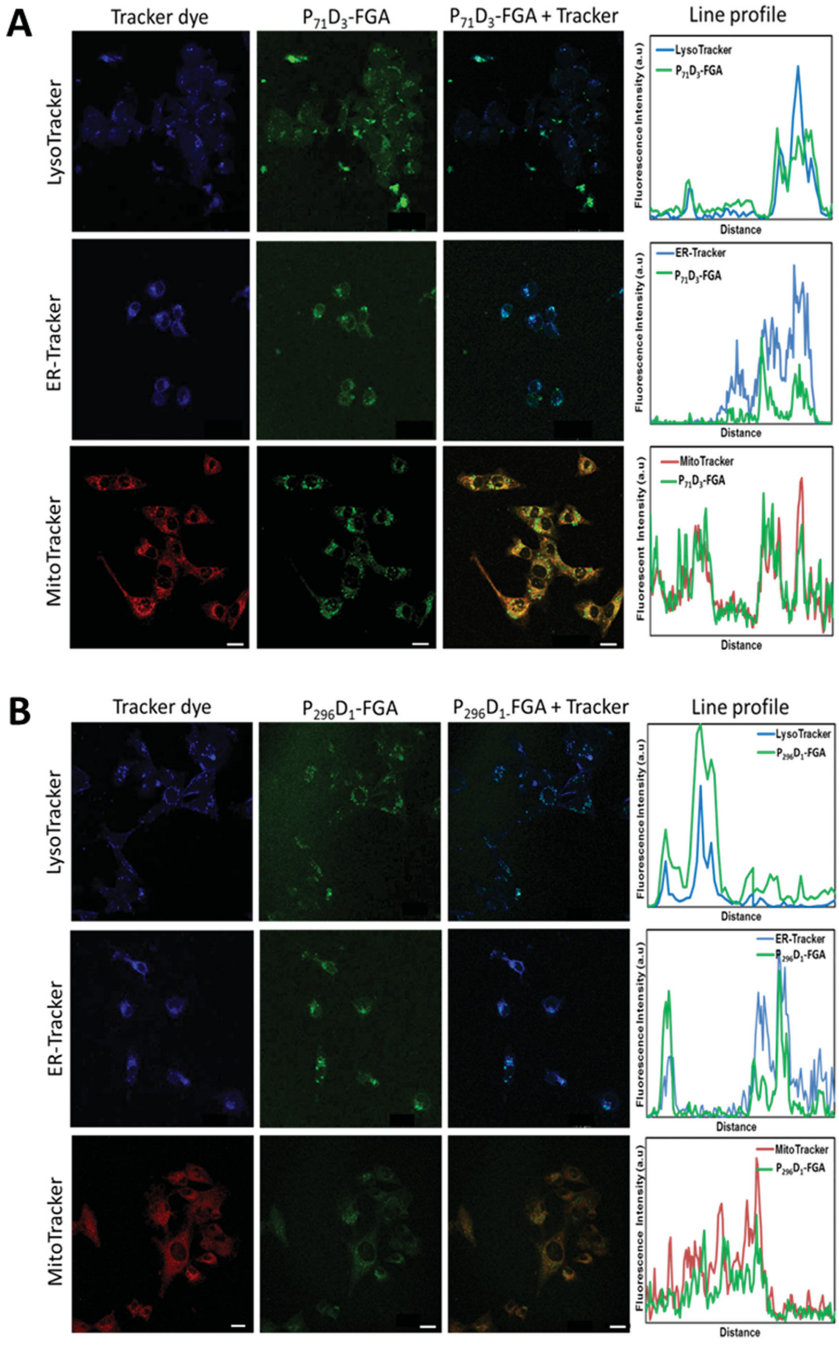

Figure 9. Cellular uptake of A) $P_{71}D_3$-FGA micelles and B) $P_{296}D_1$-FGA vesicles in MDA-MB-231 cells costained with LysoTracker, ER-Tracker, and MitoTracker. Scale bar: 20 μm.

However, colocalization of red fluorescence DOX and MitoTracker demonstrated that the DOX molecules were also localized in mitochondria after $P_{71}D_3$/DOX and $P_{296}D_1$/DOX were internalized in MDA-MB-231 cells (Figure 10A,B). Both the $P_{71}D_3$/DOX and $P_{296}D_1$/DOX demonstrated partial translocation to the endoplasmic reticulum because the FGA-labeled carrier and DOX fluorescence were partially colocalized with the ER-Tracker (Figures 9A,B and 10A,B). Conversely, free DOX showed moderate correlation with the lysosomes, endoplasmic reticulum, and mitochondria (Figure 10C), as shown by their accumulation predominantly in the nuclei (Figure 5C). These findings agree with those of Zeng et al.[28] because the polyester-based hyperbranched dendritic-linear-based nanoparticles loaded with DOX were transported to the lysosomes and mitochondria following nanocarrier endocytosis in the breast cancer MCF-7/ADR cells. Free DOX was found to be significantly colocalized with LysoTracker, whereas weak correlations were observed with the endoplasmic reticulum and mitochondria.[28]

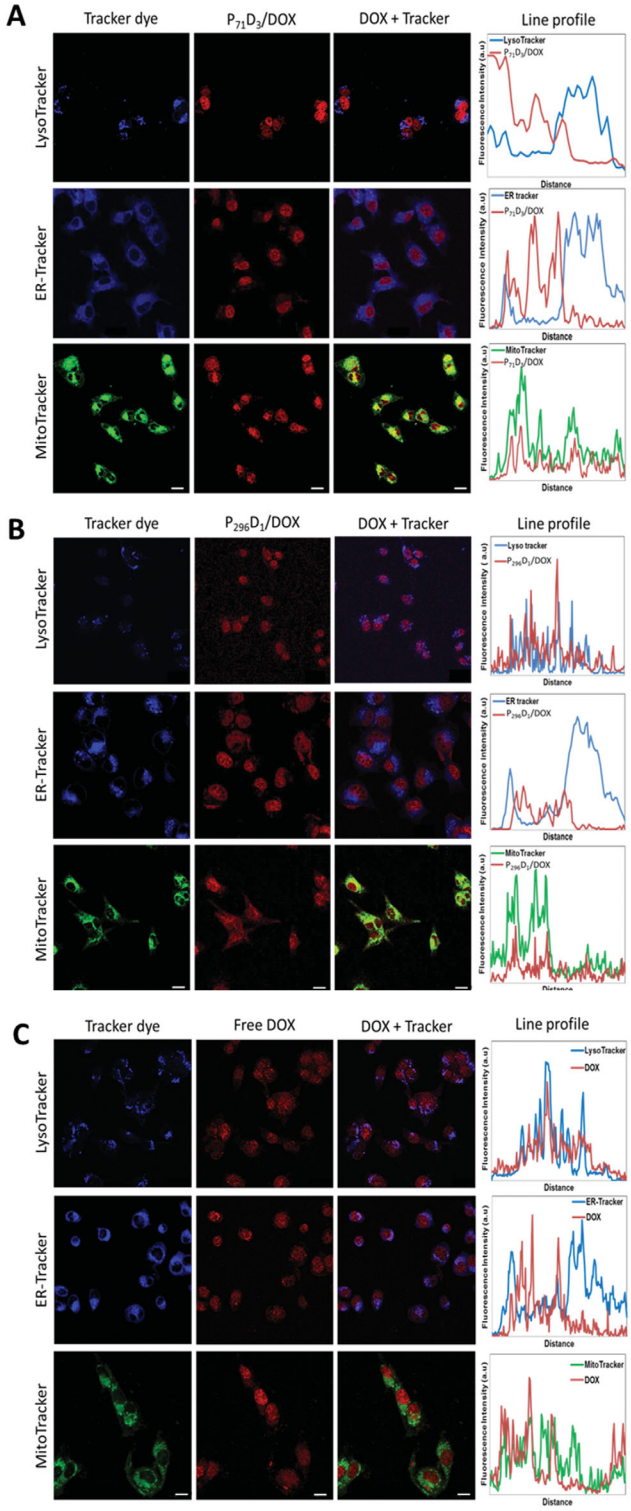

Figure 10. Cellular uptake of A) $P_{71}D_3$-FGA/DOX micelles, B) $P_{296}D_1$-FGA/DOX vesicles, and C) free DOX in MDA-MB-231 cells costained with LysoTracker, ER-Tracker, and MitoTracker. Scale bar: 20 μm.

The intracellular localization of the $P_{71}D_3$ and $P_{296}D_1$ was determined by evaluating 1 μm thick image slices of the MDA-MB-231 cell monolayer that were stacked and analyzed, together with cross-sectional slices perpendicular to the plane of the cell monolayer midpoint (*z*-axis). The *z*-slices showed that distinct FGA-labeled $P_{71}D_3$ and $P_{296}D_1$ were present in different planes throughout the thickness of the monolayer (Figure 11). Cross-sectional slices confirmed that the diblock copolymer carriers were indeed inside the cells and were not adsorbed on the outer cell surface.

4. Conclusions

In summary, this study showed that the self-assemblies of the amphiphilic diblock copolymers $P_{71}D_3$ and $P_{296}D_1$ lead to high drug (DOX) loading and that this loading was especially high in the $P_{71}D_3$ polymer micelles compared with the $P_{296}D_1$ vesicles. Small size can enable the selective accumulation of nanocarriers in tumor tissue. DOX entrapped in nanocarriers also reduces nonspecific tissue toxicity and enhances anticancer efficacy. Further conjugation with targeted ligands may give the DOX-loaded nanoparticle active targeting properties.

In comparison, the $P_{71}D_3$/DOX micelles were able to entrap ≈10 times more of the DOX compared with the other polymeric micelles, although the particle sizes were similar.[27,29] This phenomenon is the result of the bulky hydrophobic dendron pendant side chain, which forms a micelle core with a large void volume for encapsulating drugs. In terms of stability, the $P_{71}D_3$/DOX micelles exhibited higher stability, with ≈20% of the DOX being released after 48 h, whereas other polymeric micelle systems, such as poly(ethylene glycol) derivative micelles, dextran-*b*-poly(DL-lactide-*co*-glycolide) copolymer micelles and stearic acid-grafted chitosan oligosaccharide micelles, showed an average DOX release of 50% after 8 h.[27,29,30] However, the net release from the $P_{71}D_3$/DOX micelles was still four times higher than that from previously reported polymer micelles due to the loading of tenfold higher amounts of DOX in the former. This delayed release can reduce premature and undesirable DOX release into the blood circulation and allowed more $P_{71}D_3$/DOX micelles to be taken up into the tumor cells.

It is pertinent to note that the $P_{71}D_3$/DOX micelle is distinct from other micelle systems because it showed enhanced DOX accumulation in the nucleus instead of the cytoplasm and higher cytotoxicity compared with free DOX. This is in contrast to previous reports, in which free DOX showed higher accumulation in the nucleus and was more cytotoxic than the DOX-loaded stearic acid-grafted chitosan oligosaccharide micelles or PEG-poly(glutamic acid)$_2$ copolymer micelles.[31] Furthermore, the $P_{71}D_3$-FGA/DOX micelles were capable of developing into theranostic nanoparticles that can be viewed using novel imaging probes, such as photoacoustic imaging.[32]

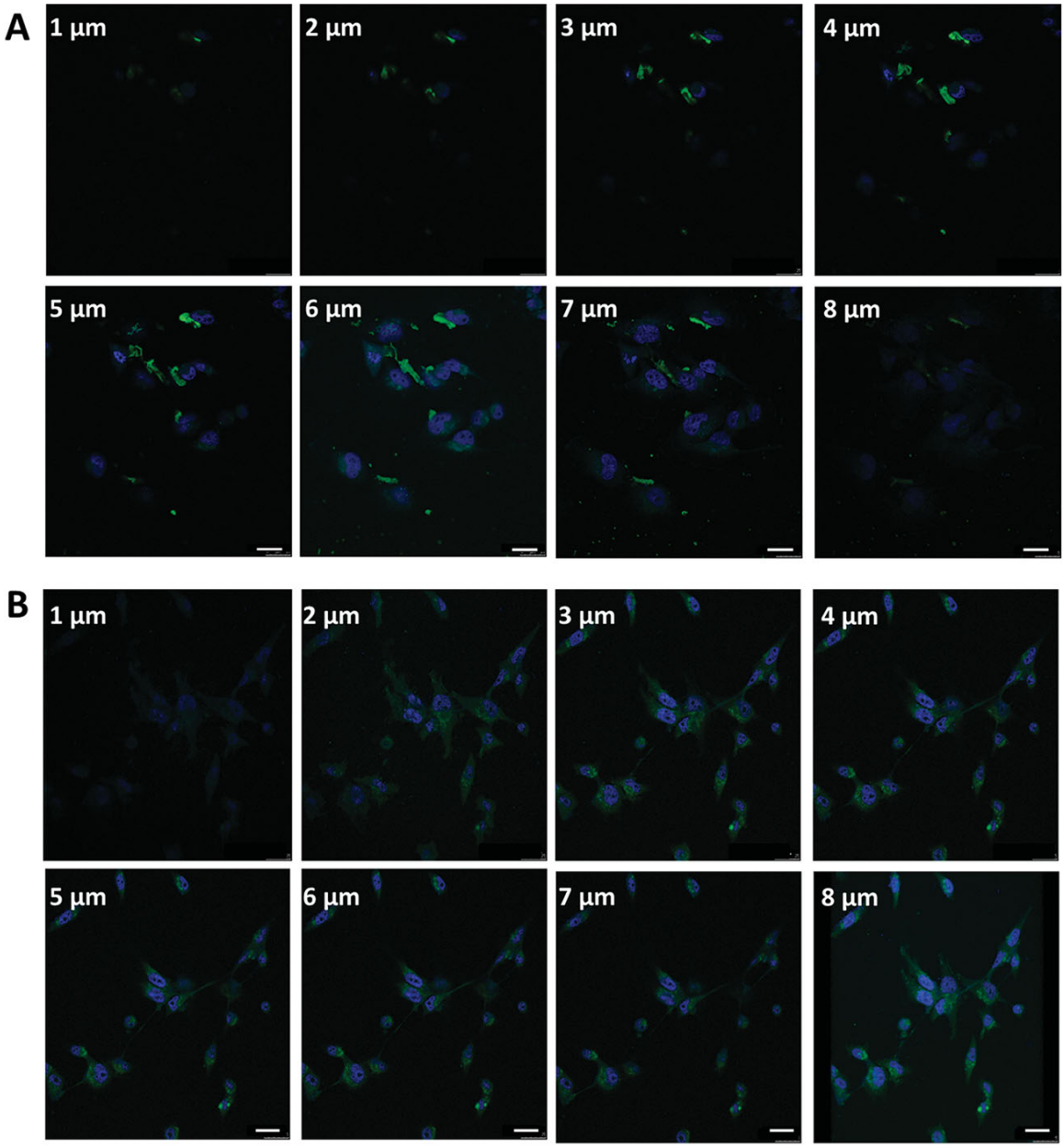

Figure 11. Z-stack confocal microscopic images of MDA-MB-231 cells incubated for 3 h with FGA-labeled nanocarriers. A) $P_{71}D_3$ micelles and B) $P_{296}D_1$ vesicles. The *z*-series were from the top to the bottom of the cell, and each slice thickness was 1 µm. The distance from the start of the *z*-stack is shown at the top left of each image. The nuclei were stained blue (DAPI). Scale bar: 20 µm.

This property could be useful in clinics to detect tumor locations and to assess therapeutic effects.

Acknowledgements: G.V., Y.-H.H., and S.H.V. contributed equally to this work. This bilateral collaborative research program was supported by the Malaysian Ministry of Higher Education's HIR-MoHE grants (UM.C/625/1/HIR/MOHE/MED/17 and UM.C/625/1/HIR/MOHE/MED/33). A.S. was financially supported by the Ministry of Science and Technology, Taiwan. S.H.V. is a recipient of the MyPhD scholarship, Ministry of Higher Education, Malaysia.

Received: November 27, 2015; Revised: January 7, 2016; Published online: February 22, 2016; DOI: 10.1002/mabi.201500435

Keywords: cellular uptake; diblock copolymer micelles; pendant dendron; self-assemblies; subcellular localization

[1] a) P. Couvreur, F. Puisieux, *Adv. Drug Delivery Rev.* **1993**, *10*, 141; b) D. D. Lasic, *Nature* **1996**, *380*, 561; c) R. Jalil, J. R. Nixon, *J. Microencapsulation* **1990**, *7*, 297; d) Z. Ahmad, A. Shah, M. Siddiq, H.-B. Kraatz, *RSC Adv.* **2014**, *4*, 17028.

[2] R. Trivedi, U. B. Kompella, *Nanomedicine* **2010**, *5*, 485.
[3] a) A. J. Windebank, M. D. Blexrud, P. C. de Groen, *J. Pharmacol. Exp. Ther.* **1994**, *268*, 1051; b) J. D. Adams, K. P. Flora, B. R. Goldspiel, J. W. Wilson, S. G. Arbuck, R. Finley, *J. Natl. Cancer Inst. Monogr.* **1993**, *15*, 141; c) M. Kongshaug, L. S. Cheng, J. Moan, C. Rimington, *Int. J. Biochem.* **1991**, *23*, 473; d) M. S. Huttel, A. Schou Olesen, E. Stoffersen, *Br. J. Anaesth.* **1980**, *52*, 77; e) J. Watkins, W. A. Milford, N. Appleyard, *Br. Med. J.* **1977**, *2*, 1084.
[4] R. A. Firestone, *Bioconjugate Chem.* **1994**, *5*, 105.
[5] S. H. Voon, L. V. Kiew, H. B. Lee, S. H. Lim, M. I. Noordin, A. Kamkaew, K. Burgess, L. Y. Chung, *Small* **2014**, *10*, 4993.
[6] a) K. Miyata, R. J. Christie, K. Kataoka, *React. Funct. Polym.* **2011**, *71*, 227; b) U. Kedar, P. Phutane, S. Shidhaye, V. Kadam, *Nanomedicine* **2010**, *6*, 714.
[7] S. Kim, Y. Shi, J. Y. Kim, K. Park, J. X. Cheng, *Expert Opin. Drug Delivery* **2010**, *7*, 49.
[8] B. Charleux, G. Delaittre, J. Rieger, F. D'Agosto, *Macromolecules* **2012**, *45*, 6753.
[9] S.-i. Yusa, Y. Shimada, T. Imae, Y. Morishima, *Polym. Chem.* **2011**, *2*, 1815.
[10] a) K. Tamano, T. Imae, S. Yusa, Y. Shimada, *J. Phys. Chem. B* **2005**, *109*, 1226; b) K. Tamano, T. Tanaka, K. Awaga, T. Imae, S.-i. Yusa, Y. Shimada, *Macromol. Rapid Commun.* **2006**, *27*, 1764.
[11] K. Osawa, T. Imae, M. Ujihara, A. Harada, K. Ochi, K. Ishihara, S.-i. Yusa, *J. Polym. Sci., Part A: Polym. Chem.* **2013**, *51*, 4923.
[12] a) T. Yamazaki, T. Imae, *J. Nanosci. Nanotechnol.* **2005**, *5*, 1066; b) T. Imae, S.-I. Hamaguchi, *Carbohydr. Polym.* **2012**, *88*, 352.
[13] A. Siriviriyanun, M. Popova, T. Imae, L. V. Kiew, C. Y. Looi, W. F. Wong, H. B. Lee, L. Y. Chung, *Chem. Eng. J.* **2015**, *281*, 771.
[14] M. Zeisser-Labouèbe, N. Lange, R. Gurny, F. Delie, *Int. J. Pharm.* **2006**, *326*, 174.
[15] L. V. Kiew, S. K. Cheong, K. Sidik, L. Y. Chung, *Int. J. Pharm.* **2010**, *391*, 212.
[16] a) J. Busquets, F. Del Galdo, E. Y. Kissin, S. A. Jimenez, *Rheumatology* **2010**, *49*, 1069; b) J. Fan, H. Park, S. Tan, M. Lee, *PLoS One* **2013**, *8*, e72474.
[17] S. H. Lim, C. Thivierge, P. Nowak-Sliwinska, J. Han, H. vanden Bergh, G. Wagnieres, K. Burgess, H. B. Lee, *J. Med. Chem.* **2010**, *53*, 2865.
[18] J. L. Misset, V. Dieras, G. Gruia, H. Bourgeois, E. Cvitkovic, S. Kalla, L. Bozec, P. Beuzeboc, C. Jasmin, J. P. Aussel, A. Riva, N. Azli, P. Pouillart, *Ann. Oncol.* **1999**, *10*, 553.
[19] K. P. Davy, D. R. Seals, *J. Appl. Physiol.* **1994**, *76*, 2059.
[20] a) I. F. Tannock, D. Rotin, *Cancer Res.* **1989**, *49*, 4373; b) Q. Wang, L. Zhou, L. Qiu, D. Lu, Y. Wu, X.-B. Zhang, *Analyst* **2015**, *140*, 5563.
[21] a) S. W. An, P. N. Thirtle, R. K. Thomas, F. L. Baines, N. C. Billingham, S. P. Armes, J. Penfold, *Macromolecules* **1999**, *32*, 2731; b) W. Groenewegen, A. Lapp, S. U. Egelhaaf, J. R. C. vander Maarel, *Macromolecules* **2000**, *33*, 4080; c) A. S. Lee, V. Bütün, M. Vamvakaki, S. P. Armes, J. A. Pople, A. P. Gast, *Macromolecules* **2002**, *35*, 8540.
[22] a) L. Smith, M. B. Watson, S. L. O'Kane, P. J. Drew, M. J. Lind, L. Cawkwell, *Mol. Cancer Ther.* **2006**, *5*, 2115; b) V. Gouaze-Andersson, J. Y. Yu, A. J. Kreitenberg, A. Bielawska, A. E. Giuliano, M. C. Cabot, *Biochim. Biophys. Acta* **2007**, *1771*, 1407; c) S. Aroui, N. Ram, F. Appaix, M. Ronjat, A. Kenani, F. Pirollet, M. DeWaard, *Pharm. Res.* **2009**, *26*, 836; d) A. Wu, K. Loutherback, G. Lambert, L. Estévez-Salmerón, T. D. Tlsty, R. H. Austin, J. C. Sturm, *Proc. Natl. Acad. Sci. USA* **2013**, *110*, 16103; e) K. Shroff, E. Kokkoli, *Langmuir* **2012**, *28*, 4729.
[23] C. F. Thorn, C. Oshiro, S. Marsh, T. Hernandez-Boussard, H. McLeod, T. E. Klein, R. B. Altman, *Pharmacogenet. Genomics* **2011**, *21*, 440.
[24] a) K. T. Thurn, H. Arora, T. Paunesku, A. Wu, E. M. B. Brown, C. Doty, J. Kremer, G. Woloschak, *Nanomedicine* **2011**, *7*, 123; b) L. Kou, J. Sun, Y. Zhai, Z. He, *Asian J. Pharm. Sci.* **2013**, *8*, 1.
[25] Y. Y. Diao, H. Y. Li, Y. H. Fu, M. Han, Y. L. Hu, H. L. Jiang, Y. Tsutsumi, Q. C. Wei, D. W. Chen, J. Q. Gao, *Int. J. Nanomed.* **2011**, *6*, 1955.
[26] T. Wei, C. Chen, J. Liu, C. Liu, P. Posocco, X. Liu, Q. Cheng, S. Huo, Z. Liang, M. Fermeglia, S. Pricl, X.-J. Liang, P. Rocchi, L. Peng, *Proc. Natl. Acad. Sci. USA* **2015**, *112*, 2978.
[27] C. Cui, Y.-N. Xue, M. Wu, Y. Zhang, P. Yu, L. Liu, R.-X. Zhuo, S.-W. Huang, *Biomaterials* **2013**, *34*, 3858.
[28] X. Zeng, R. Morgenstern, A. M. Nyström, *Biomaterials* **2014**, *35*, 1227.
[29] Y. I. Jeong, H. Kim do, C. W. Chung, J. J. Yoo, K. H. Choi, C. H. Kim, S. H. Ha, D. H. Kang, *Int. J. Nanomed.* **2011**, *6*, 1415.
[30] Y.-Q. Ye, F.-L. Yang, F.-Q. Hu, Y.-Z. Du, H. Yuan, H.-Y. Yu, *Int. J. Pharm.* **2008**, *352*, 294.
[31] a) X. B. Xiong, A. Mahmud, H. Uludag, A. Lavasanifar, *Pharm. Res.* **2008**, *25*, 2555; b) B. Sui, H. Xu, J. Jin, J. Gou, J. Liu, X. Tang, Y. Zhang, J. Xu, H. Zhang, X. Jin, *Molecules* **2014**, *19*, 11915.
[32] a) M. Mehrmohammadi, S. J. Yoon, D. Yeager, S. Y. Emelianov, *Curr. Mol. Imaging* **2013**, *2*, 89; b) Q. Zhang, N. Iwakuma, P. Sharma, B. M. Moudgil, C. Wu, J. McNeill, H. Jiang, S. R. Grobmyer, *Nanotechnology* **2009**, *20*, 395102.